Chemical Science

EDGE ARTICLE

View Article Online
View Journal | View Issue

Cite this: *Chem. Sci.*, 2017, **8**, 631

Targeting cancer cell metabolism with mitochondria-immobilized phosphorescent cyclometalated iridium(III) complexes†

Jian-Jun Cao,[a] Cai-Ping Tan,*[a] Mu-He Chen,[a] Na Wu,[a] De-Yang Yao,[b] Xing-Guo Liu,[b] Liang-Nian Ji[a] and Zong-Wan Mao*[a]

Received 1st July 2016
Accepted 22nd August 2016

DOI: 10.1039/c6sc02901a

www.rsc.org/chemicalscience

Cancer cell metabolism is reprogrammed to sustain the high metabolic demands of cell proliferation. Recently, emerging studies have shown that mitochondrial metabolism is a potential target for cancer therapy. Herein, four mitochondria-targeted phosphorescent cyclometalated iridium(III) complexes have been designed and synthesized. Complexes **2** and **4**, containing reactive chloromethyl groups for mitochondrial fixation, show much higher cytotoxicity than complexes **1** and **3** without mitochondria-immobilization properties against the cancer cells screened. Further studies show that complexes **2** and **4** induce caspase-dependent apoptosis through mitochondrial damage, cellular ATP depletion, mitochondrial respiration inhibition and reactive oxygen species (ROS) elevation. The phosphorescence of complexes **2** and **4** can be utilized to monitor the perinuclear clustering of mitochondria in real time, which provides a reliable and convenient method for *in situ* monitoring of the therapeutic effect and gives hints for the investigation of anticancer mechanisms. Genome-wide transcriptional analysis shows that complex **2** exerts its anticancer activity through metabolism repression and multiple cell death signalling pathways. Our work provides a strategy for the construction of highly effective anticancer agents targeting mitochondrial metabolism through rational modification of phosphorescent iridium complexes.

Introduction

The success of platinum-based drugs in the past few decades has stimulated great interest in the search for other metal-based anticancer agents.[1] Non-platinum anticancer drugs act through multiple mechanisms, different from those of platinum drugs.[2,3] These drugs are expected to have the capability to overcome platinum resistance and reduce side effects.[4,5] Very recently, organometallic iridium complexes have emerged as potential candidates for new metallo-anticancer drugs.[6] As demonstrated by Sadler and Meggers *et al.*, organometallic iridium complexes can exert their anticancer activity through multiple mechanisms, which include catalyzing cellular redox reactions[7,8] and inhibiting enzyme activities.[9,10] Additionally, cyclometalated iridium(III) complexes have rich photophysical properties, *e.g.*, high quantum yields, large Stokes shifts, long-lived luminescence, good photostability and cell permeability. They have attracted increasing attention in bioimaging and biosensing applications.[11–15] Our group has endeavoured to combine the unique photophysical and anticancer properties of phosphorescent cyclometalated Ir(III) complexes to construct novel multifunctional theranostic platforms that can induce and monitor the therapeutic response simultaneously.[16–19]

The central metabolic pathways operating in malignant cells are different from those in normal cells.[20,21] The alteration in cancer cell metabolism is important for oncogene revolution, tumorigenesis and tumour cell proliferation.[22–24] Compared with their normal counterparts, tumour cells are characterized by a metabolic phenotype with a shift from ATP generation through oxidative phosphorylation to ATP generation through glycolysis even under normal oxygen concentrations.[20] As mitochondria have well-recognized roles in the production of ATP and the intermediates needed for macromolecule biosynthesis, targeting mitochondria metabolism has emerged as a very effective strategy to kill cancer cells selectively.[25]

Mitochondria also play a vital role in a variety of cellular processes, such as cell death regulation, calcium modulation and redox signalling.[26,27] Cancer cells exhibit various degrees of alterations to mitochondrial function, *e.g.*, a higher

[a]*MOE Key Laboratory of Bioinorganic and Synthetic Chemistry, School of Chemistry and Chemical Engineering, Sun Yat-Sen University, Guangzhou 510275, P. R. China. E-mail: tancaip@mail.sysu.edu.cn; cesmzw@mail.sysu.edu.cn*

[b]*Key Laboratory of Regenerative Biology, Guangdong Provincial Key Laboratory of Stem Cell and Regenerative Medicine, South China Institute for Stem Cell Biology and Regenerative Medicine, Guangzhou Institutes of Biomedicine and Health, Chinese Academy of Sciences, Guangzhou, People's Republic of China*

† Electronic supplementary information (ESI) available: Experimental procedures, figures and tables, references and X-ray crystallographic data. CCDC 1452036–1452038. For ESI and crystallographic data in CIF or other electronic format see DOI: 10.1039/c6sc02901a

mitochondrial membrane potential (MMP) and increased oxidative stress, which provides opportunities to target cancer cell mitochondria for an optimal therapeutic outcome.[28]

Moreover, there has been growing interest in developing emissive mitochondria-targeted multifunctional theranostic agents that can monitor changes in the mitochondrial physiological status during the therapeutic process.[17,29,30] However, reports elucidating the consequence of targeting anticancer metal complexes to mitochondria are limited.[31,32]

In this work, four cyclometalated iridium(III) complexes, $[Ir(N\text{–}C)_2(N\text{–}N)](PF_6)$ (N–N = (2,2′-bipyridine)-4,4′-diyldimethanol ($\mathbf{L_1}$) or 4,4′-bis(chloromethyl)-2,2′-bipyridine ($\mathbf{L_2}$); N–C = 2-phenylpyridine (**ppy**) or 2-(2,4-difluorophenyl)pyridine (**dfppy**)), were designed and synthesized (Scheme 1). Due to their positive charge and lipophilicity, **1–4** were anticipated to accumulate in mitochondria. The reactive chloromethyl subunits were expected to immobilize **2** and **4** within mitochondria as the result of nucleophilic substitution with reactive thiols present in various mitochondrial proteins.[33,34] Complexes **1** and **3** incorporating non-reactive hydroxymethyl groups were used as controls. The *in vitro* antiproliferative activities of **1–4** were investigated against several cancer cell lines as well as a human normal cell line. The anticancer properties of the mitochondria-immobilized complexes **2** and **4**, which included mitochondrial damage, cellular ATP depletion, inhibition of mitochondrial respiration, reactive oxygen species (ROS) elevation and induction of apoptosis, were explored using a variety of methods. Time-dependent tracking of the mitochondrial morphology was carried out for **2**- and **4**-treated cells. Additionally, the possible anticancer mechanisms of complex **2** were elucidated by analysis of genome-wide gene expression profiles.

Results and discussion

Synthesis, characterization and stability

Complexes **1–4** were obtained by refluxing two equivalents of ligands and the corresponding cyclometalated Ir(III) dimers in CH_2Cl_2/CH_3OH (1 : 1, v/v) followed by anion exchange with NH_4PF_6 and purification by column chromatography on silica gel. Pure products of **1–4** obtained in high yields by recrystallization were characterized by ^{1}H NMR spectroscopy (Fig. S1–S4†), ESI-MS and elemental analysis (ESI†). Complexes **1**, **3** and **4** were characterized by X-ray crystallography (Fig. 1, Tables S1 and S2†). The Ir atoms have a distorted octahedral coordination

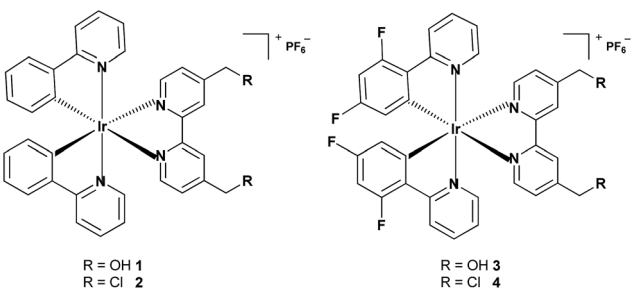

Scheme 1 Chemical structures of complexes **1–4**.

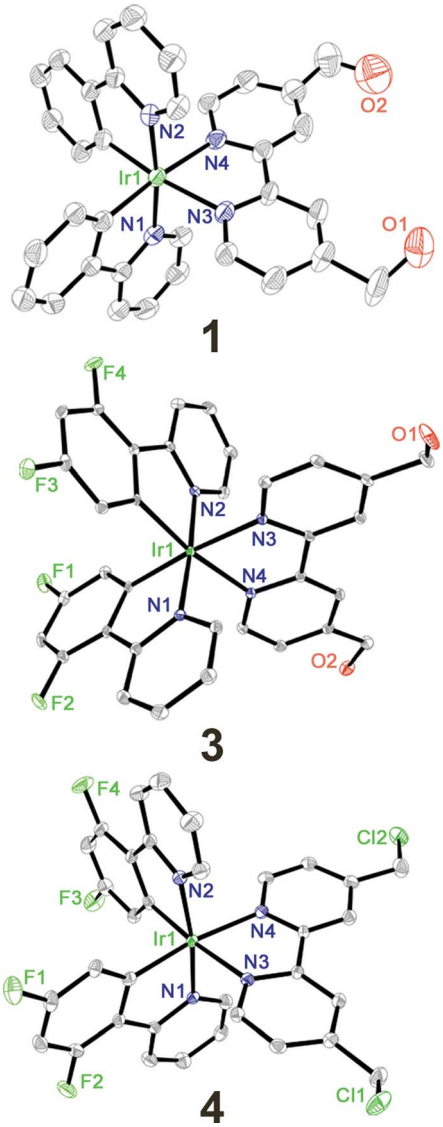

Fig. 1 X-ray crystal structures and atom-numbering schemes for complexes **1**, **3** and **4** at a 30% thermal ellipsoids probability level. The hydrogen atoms, counter ions and solvents are omitted for clarity.

geometry and the largest deviation is represented by the bite angle (from 76.4° to 76.9°) of the bipyridine ligand. The two Ir–C bonds are in a mutual *cis* arrangement, and their high *trans* influence renders slightly shorter Ir–N bond lengths in the C–N ligands than those in the cyclometalating N–N ligands. These findings are commonly observed for related cyclometalated Ir(III) complexes.[18,35]

The absorption spectra of complexes **1–4** in phosphate buffer saline (PBS), CH_3CN and CH_2Cl_2 are characterized by multiple bands (Fig. 2A and S5†). The high-energy bands (<350 nm) are assigned to spin-allowed ligand-centered (^{1}LC) π–π* transitions for cyclometalated (C–N) and ancillary (N–N) ligands. The relatively low-energy bands can be assigned to the mixed singlet and triplet metal-to-ligand charge-transfer (^{1}MLCT and ^{3}MLCT) and ligand-to-ligand charge-transfer (LLCT) transitions.[11,18,36] Upon excitation at 405 nm, complexes **1–4** exhibit long-lived

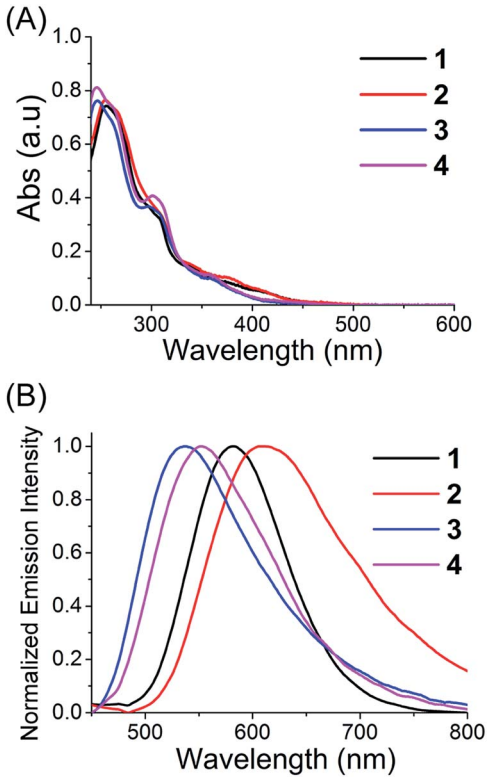

Fig. 2 (A) UV/Vis spectra of complexes **1–4** measured in CH_3CN at 25 °C. (B) Emission spectra of complexes **1–4** measured in CH_3CN at 25 °C. The excitation wavelength is 405 nm.

green to red phosphorescence (Fig. 2B, S6 and Table S3†). The emission lifetimes of **1–4** in PBS, CH_3CN and CH_2Cl_2 fall in the range between 32 and 327 ns, indicating the phosphorescent nature of the emissions. The emission lifetimes and quantum yields of **1–4** are sensitive to solvent polarity. Generally, the emission quantum yields and lifetimes of **1–4** increase upon decreasing the solvent polarity, which is also observed for other related phosphorescent Ir(III) complexes.[37]

As the reactive chloromethyl groups may undergo hydrolysis in aqueous solutions, we chose complex **2** to evaluate its stability in a DMSO-d6 and D_2O mixture (v/v, 7/3) at 37 °C. The results show that about 98.5% of complex **2** is invariant after 48 h incubation at 37 °C, as verified by ^1H NMR spectroscopy (Fig. S7†). After 7 days, about 26.2% of complex **2** is transformed, which may be attributed to the hydrolysis of the chloromethyl groups.

In vitro cytotoxicity and selective killing of cancer cells

The *in vitro* cytotoxicity of complexes **1–4** and cisplatin was determined against human cervical carcinoma (HeLa), human lung carcinoma (A549), cisplatin-resistant A549 (A549R), human breast cancer (MDB-MA-231), human prostate carcinoma (PC3) and human normal liver (LO2) cells by a 3-(4,5-dimethylthiazol-2-yl)-2,5-diphenyltetrazolium bromide (MTT) assay after 48 h treatment. Complexes **2** and **4**, with IC_{50} values ranging from 0.2 to 1.8 μM, show much higher cytotoxicity than complexes **1**, **3** and cisplatin against all the human cancer cell lines tested (Table 1). Complexes **2** and **4** are highly cytotoxic against cisplatin-resistant A549R cells, indicating they are not cross-resistant with cisplatin.

Notably, a relatively high selectivity for cancer cells is observed for complex **2**. For example, it shows approximately an 11 fold higher selectivity for cancerous A549 cells over noncancerous LO2 cells. A co-culture model of LO2 and A549 cells was used to further demonstrate the capability of complex **2** to selectively kill cancer cells (Fig. S8†). The nuclei of A549 cells were prelabeled with Hoechst 33 342 (2′-(4-ethoxyphenyl)-5-(4-methyl-1-piperazinyl)-2,5′-bi-1*H*-benzimidazole trihydrochloride). After the cocultured cells are treated with **2**, most of the A549 cells (blue nuclei) are stained positively by both annexin V and PI, while the LO2 cells are still viable. The hyperchromatic nuclei of the A549 cells indicate that **2** mainly induces apoptotic cell death.

Lipophilicity, cellular uptake and localization

It has been reported that the cellular uptake behaviour of metal complexes is usually related to many factors, *e.g.*, lipophilicity, molecular size and substitute groups.[18,38,39] The lipophilicity is referred to as log $P_{o/w}$ (where $P_{o/w}$ = the octanol/water partition coefficient). The log $P_{o/w}$ values, determined by a classical shake-flask method, for **1**, **2**, **3** and **4** are 0.23, 1.28, 1.09 and 2.12, respectively.

As iridium is an exogenous element, the cellular uptake levels of Ir(III) can be quantitatively determined by inductively coupled plasma-mass spectrometry (ICP-MS). The cellular uptake efficacy is influenced by the lipophilicity and the substitution groups on the N–N ligand (Table S4†). It should be noted that complexes **2** and **4** with the chloromethyl substituents show a much higher cellular uptake efficacy than **1** and **3** containing the hydroxymethyl groups.

The localization of **1–4** in A549 cells was investigated by laser scanning confocal microscopy. All the complexes can be visualized in the A549 cells after 1 h incubation (Fig. S9†). The phosphorescence of **1–4** shows distinct filamentous and punctate patterns. Colocalization experiments of **1–4** with the mitochondrion-specific fluorescent probe MitoTracker Deep Red (**MTDR**) show that **1–4** can specifically localize to mitochondria (Fig. 3). The Pearson's colocalization coefficients obtained for **1–4** with **MTDR** are 0.74, 0.84, 0.87 and 0.82, respectively. Similar results are also observed for **2** and **4** by high resolution confocal scanning laser microscopy (Fig. S10†). However, negligible colocalization of **1–4** with LysoTracker Deep Red (**LTDR**) can be detected (Fig. S11†). To further verify the distribution of **1–4** in different cellular compartments, the mitochondrial, cytosolic and nuclear fractions were isolated from A549 cells treated with complexes **1–4** (Fig. S12†). As measured by ICP-MS, the content of iridium in the mitochondria is much higher than that obtained in the cytosol and nuclei. These results collectively indicate that complexes **1–4** can specifically target mitochondria in A549 cells.

We further investigated the cellular uptake mechanisms of **1–4**. Incubation of A549 cells with **1–4** at a lower temperature

Table 1 Cytotoxicity of the tested compounds against different cell lines

Compounds	IC_{50}[a] (μM)					
	HeLa	A549	A549R	MDB-MA-231	PC3	LO2
1	10.0 ± 0.9	24.0 ± 2.0	42.2 ± 2.7	24.5 ± 1.9	>100	>100
2	0.52 ± 0.04	0.40 ± 0.02	0.64 ± 0.04	0.33 ± 0.02	1.4 ± 0.1	4.5 ± 0.3
3	2.7 ± 0.2	16.8 ± 1.2	17.8 ± 1.4	12.3 ± 1.1	38.0 ± 1.9	8.1 ± 0.5
4	1.8 ± 0.1	0.21 ± 0.02	0.74 ± 0.05	0.66 ± 0.05	1.04 ± 0.09	1.5 ± 0.1
Cisplatin	18.8 ± 1.4	22.4 ± 2.0	120.2 ± 6.5	27.5 ± 2.5	23.8 ± 2.0	26.9 ± 1.9

[a] Cells were incubated with the indicated compounds for 48 h. Data are presented as the means ± standard deviations (SD), and cell viability was assessed after 48 h of incubation.

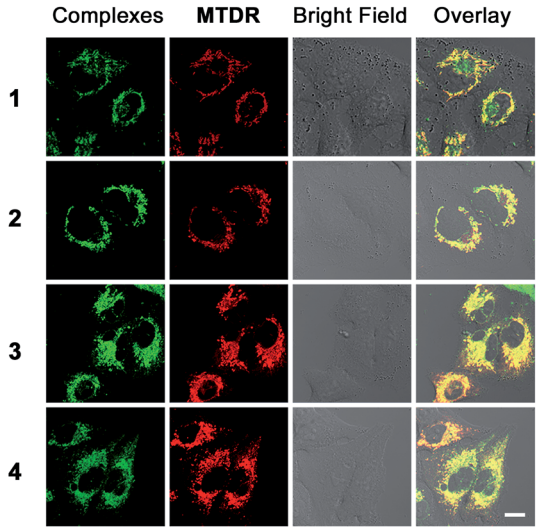

Fig. 3 Determination of colocalization of **1–4** with MTDR by confocal microscopy. A549 cells were incubated with **1–4** (10 μM, 1 h), and then stained with MTDR (100 nM, 30 min) at 37 °C. **1** and **2**: λ_{ex} = 405 nm; λ_{em} = 630 ± 20 nm. **3** and **4**: λ_{ex} = 405 nm; λ_{em} = 560 ± 20 nm. MTDR: λ_{ex} = 633 nm, λ_{em} = 655 ± 20 nm. Scale bar: 10 μm.

(4 °C) results in a reduced cellular uptake efficiency as revealed by confocal microscopy (Fig. S13–16†). Pretreatment of the cells with metabolic inhibitors, 2-deoxy-D-glucose and oligomycin, can lower the cellular uptake levels of these complexes, while the endocytosis modulator chloroquine shows no effect on the ability of complexes to cross the plasma membrane. The results suggest that complexes **1–4** penetrate the cell membrane mainly through an energy-dependent mechanism and do not rely on the endocytic pathways.[40]

Mitochondrial immobilization

As complexes **2** and **4** contain chloromethyl groups, they are supposed to react with thiol groups of cysteine residues in proteins and peptides in cells to form stable covalent bonds.[34] MitoTracker™ probes, commercial thiol reactive mitochondrial dyes containing chloromethyl groups, can be retained during cell fixation.[33] Similar to that observed for **MTDR**, the emission of complexes **2** and **4** is retained in cells after the cells are fixed and washed (Fig. 4). Rhodamine 123, a conventional mitochondrial dye, is easily washed out once the MMP is lost.[41] As expected, the emission of Rhodamine 123, and complexes **1** and **3** is barely detectable in cells under the same conditions. The higher cytotoxicity of **2** and **4** compared with **1** and **3** is correlated with their higher uptake efficacy, which may be at least partially attributed to their immobilization and prolonged retention time in mitochondria.

The ability of **1–4** to undergo covalent conjugation to intracellular proteins was also confirmed by gel electrophoresis, which separates the proteins purified under denaturing conditions from lysed A549 cells treated with Ir(III) (Fig. S17†). Distinct emissive protein bands can be observed in the gel-

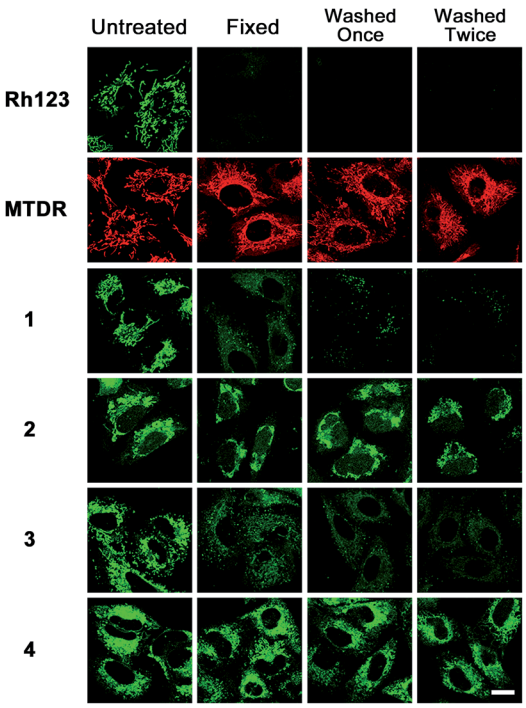

Fig. 4 Sensitivity of emission intensity of Rhodamine 123 (**Rh123**), MTDR and Ir(III) to fixation and washing. A549 cells were incubated with **1–4** (10 μM) at 37 °C for 1 h. The cells were fixed by paraformaldehyde and washed twice with PBS/DMSO (9/1, v/v). The cells were imaged by confocal microscopy after each step. **1** and **2**: λ_{ex} = 405 nm; λ_{em} = 630 ± 20 nm. **3** and **4**: λ_{ex} = 405 nm; λ_{em} = 560 ± 20 nm. Scale bar: 10 μm.

separated denatured protein mixtures isolated from **2**- and **4**-treated cells. Meanwhile, no emissive bands are detected in proteins isolated from **1**- and **3**-treated cells. Similar results are observed *in vitro* using bovine serum albumin (BSA) as a model protein that contains one free cysteine residue (Fig. S18†). The interactions of complexes **1–4** with BSA have also been investigated using tryptophan fluorescence quenching experiments (Fig. S19†). The Stern–Volmer constants (K_{SV}) determined for **1**, **2**, **3** and **4** are 7.0×10^4, 1.1×10^5, 7.2×10^4 and 8.5×10^4 M^{-1}, respectively. Accordingly, an increase in the emission intensities is observed for **1–4** upon binding with BSA (Fig. S20†). Complex **2** displays approximately an 11.6-fold emission enhancement when the molar ratio of BSA and Ir(III) reaches 8 : 1. The enhancement in emission intensities can be attributed to the hydrophobic environment in the binding pockets of proteins, which is favourable for their imaging applications.[37] These results indicate that complexes **2** and **4** can be immobilized on mitochondria by covalent interactions with proteins.

Induction of mitochondrial dysfunction

As complexes **1–4** could be localized to mitochondria, their impact on mitochondrial integrity was monitored by detecting the changes in MMP ($\Delta\Psi_m$). The red/green fluorescence of 5,5′,6,6′-tetrachloro-1,1′-3,3′-tetraethyl-benzimidazolylcarbocyanine iodide (JC-1), a mitochondria-selective aggregate dye, was detected by flow cytometry (Fig. 5A) and confocal microscopy (Fig. S21†).[42] At low membrane potentials, JC-1 exists in the form of the "J-monomer" with green fluorescence. At high membrane potentials, JC-1 forms "J-aggregates" and displays red fluorescence. The control cells show red fluorescence, which indicates that the mitochondrial membranes retain a high voltage. The capability of these complexes to depolarize mitochondria is correlated with their cytotoxicity. In cells treated with **1** and **3**, a small portion of cells lose their $\Delta\Psi_m$. Complexes **2** and **4** cause a marked decrease in MMP, as evidenced by the fluorescence shift from red to green. After a 6 h treatment, the percentage of cells with mitochondrial membrane depolarization increases from $6.6 \pm 0.7\%$ to $85.7 \pm 1.7\%$ and $82.4 \pm 7.6\%$ for **2** (10 μM, 6 h) and **4** (10 μM, 6 h), respectively.

To further investigate the effects of complexes **1–4** on the mitochondrial metabolic status, we measured their impact on the intracellular ATP level and mitochondrial respiration. The capability of **1–4** to reduce the ATP content in A549 cells is correlated with their cytotoxicity (Fig. 5B). The impact of complexes **1** and **3** on intracellular ATP levels is not obvious. Meanwhile, complexes **2** and **4** cause a significant dose-dependent decrease in ATP production as compared with the control cells. At a concentration of 10 μM, the ATP levels decrease from 86.3 ± 1.0 to 30.2 ± 2.4 and 20.2 ± 3.3 nM for **2** and **4**, respectively.

Complexes **2** and **4** were chosen as model compounds to further investigate their impact on the mitochondrial bioenergetic status. Mitochondrial respiration was quantified by measuring the oxygen consumption rate (OCR) directly using a Seahorse XF24 Extracellular Flux Analyzer.[43] Several key parameters were measured to assess mitochondrial oxidative phosphorylation (OXPHOS) by using modulators of respiration that target components of the electron transport chain (ETC) (Fig. 5C and D). Cells treated with **2** and **4** display a decrease in basal OCR (Fig. 5E). The mitochondrial respiration comprises coupled respiration for ATP synthesis and uncoupled respiration to drive the futile cycle of proton pumping and proton leak back across the inner mitochondrial membrane.[44] The coupled respiration and proton leak were determined using the ATP synthase inhibitor oligomycin. Cells treated with **2** and **4** show a dose-dependent decrease in ATP production as compared with the control cells (Fig. 5F). Proton leak is increased at a lower concentration (0.25 μM) with a decline observed at higher concentrations (1 μM) (Fig. 5G). After injection of the carbonyl cyanide 4-(trifluoromethoxy)phenylhydrazone (FCCP), a potent mitochondrial uncoupling agent that can dissipate the proton gradient and eliminate the control of respiration by ATP synthase, a decrease in the OCR peak of Ir(III)-treated cells is observed as compared with the resilient control cells. The observation suggests that the Ir(III)-treated cells have lost their spare respiratory capacity.[45] Then, a mixture of antimycin A (a mitochondrial complex III inhibitor) and rotenone (a mitochondrial complex I inhibitor), which can shut down the mitochondrial respiratory chain thoroughly, was injected to determine the fraction of non-mitochondrial O_2 consumption including substrate oxidation and cell surface oxygen consumption. A decrease in non-mitochondrial respiration is detected in cells treated with **2** and **4** (Fig. 5H). These results collectively indicate that the inhibition of both mitochondrial and non-mitochondrial respiration contributes to the cytotoxicity of **2** and **4**.

Real-time tracking of mitochondrial morphology

Mitochondria are highly dynamic organelles that undergo constant fusion and fission. Mitochondria are actively transported in cells, which is essential for maintaining physiological functions of cells.[46] However, the molecular mechanisms regulating these behaviours have not been well understood yet. Thus, tracking the changes in mitochondrial morphology may give insight into the investigation of cell death mechanisms.[47] Real-time tracking of the mitochondrial morphology was carried out by monitoring the emission of **2** and **4** in A549 cells using confocal microscopy (Fig. 6A and B). A549 cells can be effectively labelled by **2** and **4** after 0.5 h incubation, when mitochondria show the normal tubular network and distribution. Prolonged incubation causes a collapse of the normal tubular mitochondrial network into mitochondrial aggregates and large perinuclear clusters. Mitochondrial swelling, fragmentation and perinuclear clustering in cells treated with **2** and **4** are also confirmed by transmission electron microscopy (TEM, Fig. 6C). It can be seen that in control cells, mitochondria are distributed evenly in the cytoplasm. In Ir(III)-treated cells, the fragmented mitochondria tend to localize around the nucleus.

Intracellular ROS detection

Apart from producing energy, mitochondria are also a major source of ROS. Mitochondrial damage and intracellular ROS production are closely related.[27] Intracellular ROS elevation induced by complexes **1–4** was detected by flow cytometry and

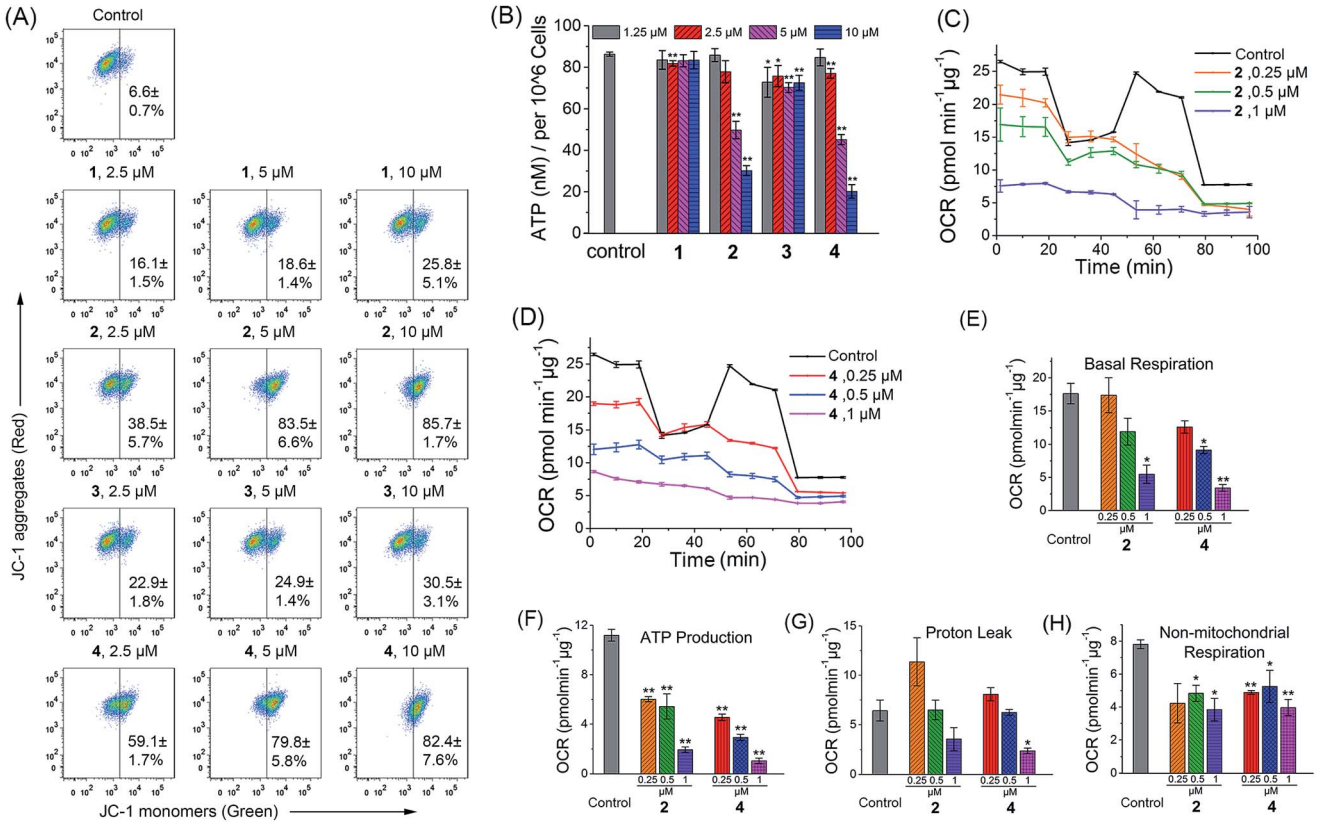

Fig. 5 Induction of mitochondrial dysfunction by complexes **1**–**4**. (A) Effects of **1**–**4** on MMP analyzed by flow cytometry at the indicated concentrations. A549 cells were treated for 6 h then stained with JC-1. λ_{ex} = 488 nm. λ_{em} = 530 ± 30 nm (green) and 585 ± 30 nm (red). (B) Intracellular ATP levels in A549 cells. The cells were treated with the vehicle and **1**–**4** at the indicated concentrations for 6 h. (C and D) Respiratory profiles of control and **2**- and **4**-treated A549 cells under basal conditions, and after the addition of oligomycin (0.75 μM), FCCP (0.6 μM) and the mixture of rotenone (0.5 μM) and antimycin A (0.5 μM) measured by a Seahorse XF24 Extracellular Flux Analyzer. The OCR values were normalized to 1 μg protein determination by the BCA assay. (E) Basal respiration was calculated by subtracting OCR values after the addition of the mixture of rotenone (0.5 μM) and antimycin A (0.5 μM) from basal OCR. (F) ATP production was calculated by subtracting OCR values after the addition of oligomycin from basal OCR. (G) Proton leak was calculated by subtracting OCR values after the addition of the mixture of rotenone (0.5 μM) and antimycin A (0.5 μM) from OCR values obtained after the addition of oligomycin. (H) Non-mitochondrial respiration was the OCR value after the addition of the mixture of rotenone (0.5 μM) and antimycin A (0.5 μM). *p < 0.05, **p < 0.01.

confocal microscopy with 2′,7′-dichlorodihydrofluorescein diacetate (H_2DCFDA) staining. H_2DCFDA can be converted to the highly fluorescent 2′,7′-dichlorofluorescein (DCF) by cellular ROS.[48] After a 6 h treatment, a dramatic concentration-dependent ROS elevation is observed for **2**- and **4**-treated A549 cells. At a concentration of 10 μM, treatment with **2** and **4** increases the mean fluorescent intensity (MFI) by approximately 5.5- and 13.7-fold, respectively (Fig. 7). Similar results are also obtained by confocal microscopy, with markedly concentration-dependent increases in the intensity of the DCF fluorescence observed in **2**- and **4**-treated cells (Fig. S22†). Additionally, pre-treatment of A549 cells with *N*-acetyl-L-cysteine (NAC), a ROS scavenger, significantly diminishes the antiproliferative potency of **2** and **4** (Fig. S23†). These results indicate that **2** and **4** induce ROS-dependent cell death.

Cell cycle arrest and induction of apoptosis

In addition to their role as ATP generators, mitochondria mediate essential cell functions such as cell-cycle control and apoptosis.[49] Cell cycle arrest may occur in response to the blockage of macromolecule biosynthesis caused by a lack of ATP production and mitochondrial dysfunction.[50] Mitochondria play a key role in apoptosis by regulating the release of cytochrome c and other pro-apoptotic proteins from the space between the inner and outer mitochondrial membranes to the cytosol.[26]

Cell cycle arrest in A549 cells induced by **2** and **4** was analyzed by flow cytometry using propidium iodide (PI) staining (Fig. 8A). Complexes **2** and **4** cause a dose-dependent G0/G1 cell cycle arrest. After treatment with Ir(III) for 24 h, the percentage of cells in the G0/G1 phase increases from 57.4 ± 3.1% (control) to 85.3 ± 4.4% and 88.8 ± 5.2% for **2** (2.5 μM) and **4** (2.5 μM), respectively.

The morphology of apoptotic cells is characterized by cell shrinkage, nuclear fragmentation, chromatin condensation and membrane blebbing.[51] First, the ultrastructural changes in the morphology of cells were examined by TEM (Fig. 8B). The control cells show a normal morphology. In contrast, the cells

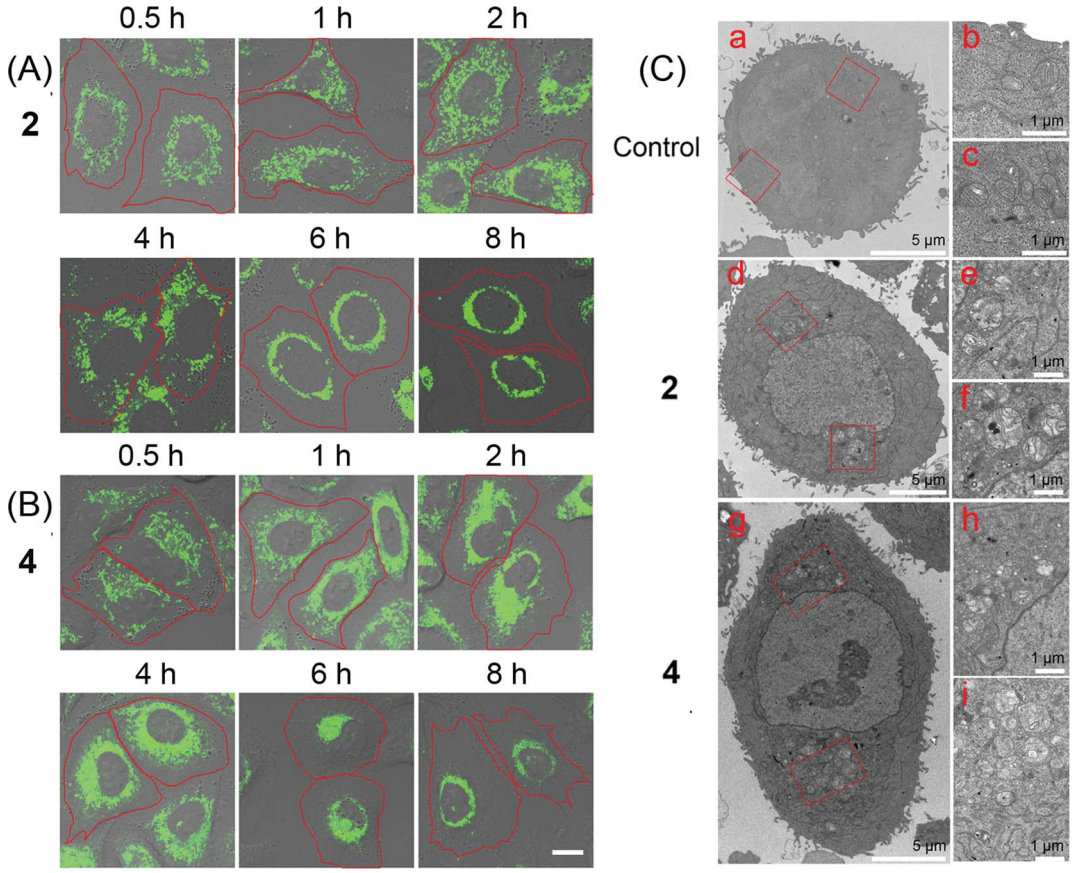

Fig. 6 (A and B) Confocal microscopic tracking of the mitochondrial morphology in real-time using **2** (10 μM) and **4** (10 μM) over a period of 8 h. **2**: $\lambda_{ex} = 405$ nm; $\lambda_{em} = 630 \pm 20$ nm. **4**: $\lambda_{ex} = 405$ nm; $\lambda_{em} = 560 \pm 20$ nm. The cell borders are recognizable and outlined with the red curve. Scale bar: 10 μm. (C) Representative TEM images showing the perinuclear clustering of abnormal swollen mitochondria of A549 cells treated with **2** (d–f) and **4** (g–i) at a concentration of 5 μM for 24 h. (b) and (c) are enlarged views of the red zones in (a). (e) and (f) are enlarged views of the red zones in (d). (h) and (i) are enlarged views of the red zones in (g).

treated with **2** and **4** show obvious morphological evidence of different stages of apoptosis including condensed chromatin, nuclear fragmentation and apoptotic bodies. In addition, similar phenomena are also observed in Ir(III)-treated A549 cells stained with Hoechst 33 342 (Fig. S24†). The control cells exhibit homogeneous nuclear staining, and the Ir(III)-treated cells display typical apoptotic changes, *e.g.*, bright staining, condensed chromatin and fragmented nuclei.

The activation of caspases is one of the best recognized biochemical hallmarks of apoptosis.[52] The effect of Ir(III) treatment on caspase-3/7 activity was determined using the Caspase-Glo assay. Treatment of A549 cells with **2** and **4** stimulates the activation of caspase-3/7 in a dose-dependent manner (Fig. S25†). After a 12 h treatment at a concentration of 10 μM, the activity of caspase-3/7 is increased by approximately 1.6- and 1.7-fold in **2**- and **4**-treated cells, respectively. Similar to that observed for cisplatin, pre-treatment of the cells with the pan-caspase inhibitor, z-VAD-fmk, inhibits the antiproliferative activity of **2** and **4** (Fig. S26†).

During apoptosis, phosphatidylserine (PS) is exposed externally due to loss of the asymmetry of plasma membrane phospholipids, and externalized phosphatidylserine emits eat-me signals to neighboring cells.[51] The percentage of apoptotic cells was determined by annexin V and PI double labeling, measured by flow cytometry (Fig. S27†) and confocal microscopy (Fig. S28†). After treatment of cells with **2** and **4** for 24 h, the percentages of cells in both the early apoptotic (annexin V-positive and PI-negative) and the late/necrotic (annexin V-positive and PI-positive) stages increase dose-dependently. After 24 h of treatment, apoptotic cells increase from 1.4 ± 0.02% to 17.5 ± 0.8% and 61.5 ± 1.1% for **2** (10 μM) and **4** (10 μM), respectively. Moreover, pre-treatment of A549 cells with NAC decreases the apoptosis-inducing capability of **2** and **4** (Fig. S27†). These results collectively indicate that **2** and **4** induce caspase-dependent and ROS-mediated apoptotic cell death.

Microarray analysis

Complex **2** shows comparable cytotoxicity to complex **4** against the cancer cells tested, while it is less cytotoxic towards normal LO2 cells. We chose complex **2** as the model compound for microarray analysis to further elucidate the underlying mechanisms. Genome-wide gene transcriptional profiles of **2**-treated cells were determined by Affymetrix human U133 plus

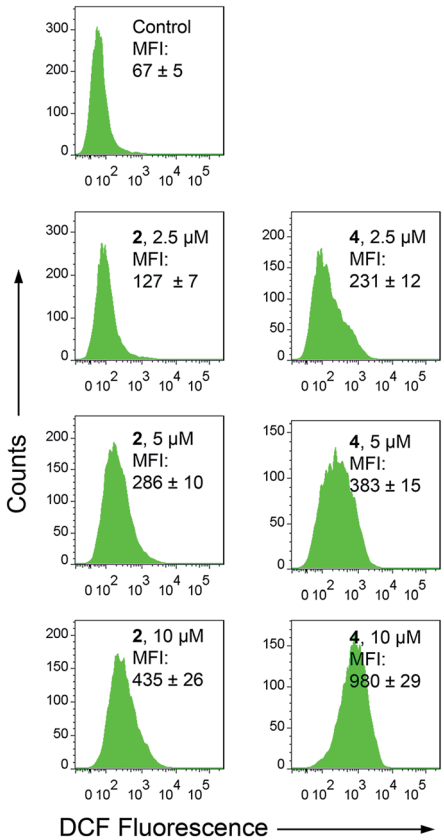

Fig. 7 Intracellular ROS production measured by DCF fluorescence (λ_{ex} = 488 nm, λ_{em} = 530 ± 30 nm) with flow cytometry. A549 cells were treated with **2** and **4** at the indicated concentrations for 6 h.

2.0 microarray analysis in triplicate runs (Table S5†). 507 gene sets are identified as being up-regulated and 715 gene sets are down-regulated by more than two-fold in **2**-treated A549 cells (Table S6†). The heat shock 70 kDa protein 6 (HSP70B′) gene, is markedly increased (about 79-fold). HSPs are anti-apoptotic proteins, their expression can be induced in response to anti-cancer chemotherapy, and HSP70 can also prevent both caspase-dependent and caspase-independent cell death.[53] The elevated expression of HSP70B′ confirms that **2** initiates apoptotic machinery in A549 cells. The mitochondrion-encoded critical subunits I, II and III of cytochrome c oxidase (COX1, COX2 and COX3) decrease significantly with up to a 15-fold decrease observed for COX1. The decrease in transcription of these genes in the respiratory chain confirms that treatment with **2** causes dysfunction of aerobic respiration.

In order to identify the possible anticancer mechanisms, a connectivity map (Cmap, http://www.broad.mit.edu/cmap/), which contains genome-wide transcriptional expression data from a panel of cell lines treated with a library of 1309 bioactive small molecules, was used to analyze the list of transcripts regulated by **2**.[55] The results of the Cmap analysis in the case of **2** are summarized in Table S7.† A high correlation is obtained with **2** and pyrvinium, which can inhibit the mitochondrial respiration.[56]

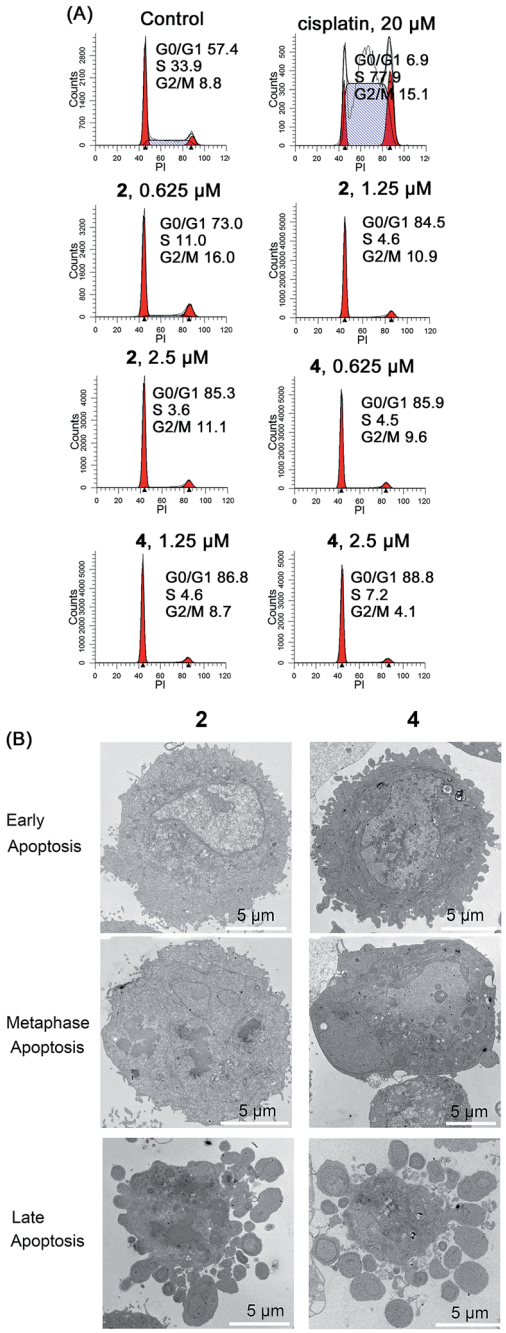

Fig. 8 (A) Effects of **2** and **4** on cell cycle distribution analyzed by flow cytometry. A549 cells were stained by PI after treatment for 24 h. (B) Representative TEM images showing different stages of apoptosis in A549 cells treated with **2** and **4** (10 μM) for 24 h.

To mine the core biological functions from the enormous dataset of a microarray, the impacted genes have been divided into three Gene Ontology (GO) database categories: biological process, cellular component and molecular function. Using the predefined gene sets by gene ontology, there are 43 pathways that are significantly enriched with the differentially expressed genes from the **2**-treated group (Table S8†). Treatment with **2** influences several important biological processes such as the mitotic cell cycle, mitotic nuclear division and DNA replication.

The regulated genes derived from microarray experiments were analyzed by a web-based bioinformatics tool, DAVID (database for annotation, visualization, and integrated discovery).[54] The modulation of cell signalling pathways by **2** is summarized in Table S9.† The results suggest that **2** affects several pathways known to regulate cell death, including the cell cycle, DNA replication and the p53 signalling pathway. The mitochondrion is a central metabolic organelle, and it executes critical functions for the metabolism of fatty acids, amino acids and nucleotides. Treatment with **2** influences metabolic pathways related to mitochondrial functions, such as D-glutamine and D-glutamate metabolism, alanine, aspartate and glutamate metabolism and pyrimidine metabolism. These findings are consistent with the experimental results.

In order to further confirm that **2**-induced cell death occurs through mitochondrial dysfunction, cell cycle perturbation and apoptosis, we validate the differential expression of 21 genes involved in several key pathways (mitochondrial metabolism, the p53 signalling pathway and the cell cycle) in response to **2**-treatment by quantitative real-time PCR (RT-PCR). The primer sequences of the selected genes studied in RT-PCR are listed in Table S10,† and the functions of these genes are listed in Table S11.† The heat map of the **2**-induced expression profile of A549 cells to the untreated control is shown in Fig. S30.† The fold changes of expression as determined by RT-PCR for these genes are concordant with those obtained by microarray analysis (Fig. S31†). Based on the results of bioinformatic analyses, the proposed anticancer mechanisms of action of **2** are depicted in Fig. S32.† The cytotoxicity of **2** is suggested to be related to mitochondrial damage, elevation of ROS, initiation of DNA damage responses, cell cycle arrest and induction of apoptosis.

Conclusions

In summary, four cyclometalated Ir(III) complexes with 4′,4′-substituted 2′,2′-bipyridyl ligands have been developed as mitochondria-targeted anticancer agents. Among them, complexes **2** and **4** containing a reactive chloromethyl group can be fixed on mitochondria through nucleophilic substitution with reactive thiols present in mitochondrial proteins. The immobilization of complexes **2** and **4** on mitochondria results in a much higher cytotoxicity than the non-fixable complexes **1** and **3**, which may attributed to their higher cellular penetration capability as well as a longer retention time on mitochondria. Mechanism studies show that **2** and **4** mainly induce caspase- and ROS-mediated apoptotic cell death. Complexes **2** and **4** can lower the intracellular ATP levels, attenuate the mitochondrial bioenergetic function and induce mitochondrial depolarization. Interestingly, complexes **2** and **4** can be also utilized to monitor mitochondrial morphological changes, which provides the possibility for *in situ* monitoring of the therapeutic effect, and gives insights into their anticancer mechanisms. Moreover, complex **2** can selectively kill cancer cells over normal cells. Overall, our work shows that targeting mitochondrial metabolism by immobilization is a very effective strategy for the construction of multifunctional phosphorescent metal complexes with enhanced anticancer activity and selectivity towards cancer cells.

Acknowledgements

This study was supported by the 973 program (no. 2014CB845604 and 2015CB856301), the National Science Foundation of China (no. 21572282, 21231007 and 21571196), the Ministry of Education of China (no. IRT1298), the Guangdong Natural Science Foundation (2015A030306023), the Science and Technology Program of Guangzhou (2014J4100140) and the Fundamental Research Funds for the Central Universities.

Notes and references

1 N. Muhammad and Z. Guo, *Curr. Opin. Chem. Biol.*, 2014, **19**, 144–153.
2 G. Gasser and N. Metzler-Nolte, *Curr. Opin. Chem. Biol.*, 2012, **16**, 84–91.
3 Z. Liu and P. J. Sadler, *Acc. Chem. Res.*, 2014, **47**, 1174–1185.
4 C. H. Leung, H. J. Zhong, D. S. H. Chan and D. L. Ma, *Coord. Chem. Rev.*, 2013, **257**, 1764–1776.
5 S. Komeda and A. Casini, *Curr. Top. Med. Chem.*, 2012, **12**, 219–235.
6 Z. Liu, A. Habtemariam, A. M. Pizarro, S. A. Fletcher, A. Kisova, O. Vrana, L. Salassa, P. C. Bruijnincx, G. J. Clarkson, V. Brabec and P. J. Sadler, *J. Med. Chem.*, 2011, **54**, 3011–3026.
7 Z. Liu, I. Romero-Canelon, B. Qamar, J. M. Hearn, A. Habtemariam, N. P. Barry, A. M. Pizarro, G. J. Clarkson and P. J. Sadler, *Angew. Chem., Int. Ed.*, 2014, **53**, 3941–3946.
8 J. J. Soldevila-Barreda and P. J. Sadler, *Curr. Opin. Chem. Biol.*, 2015, **25**, 172–183.
9 A. Wilbuer, D. H. Vlecken, D. J. Schmitz, K. Kraling, K. Harms, C. P. Bagowski and E. Meggers, *Angew. Chem., Int. Ed.*, 2010, **49**, 3839–3842.
10 C. H. Leung, H. J. Zhong, H. Yang, Z. Cheng, D. S. Chan, V. P. Ma, R. Abagyan, C. Y. Wong and D. L. Ma, *Angew. Chem., Int. Ed.*, 2012, **51**, 9010–9014.
11 C. Y. Li, M. X. Yu, Y. Sun, Y. Q. Wu, C. H. Huang and F. Y. Li, *J. Am. Chem. Soc.*, 2011, **133**, 11231–11239.
12 L. C. Lee, J. C. Lau, H. W. Liu and K. K. Lo, *Angew. Chem., Int. Ed.*, 2016, **55**, 1046–1049.
13 X. Ma, J. Jia, R. Cao, X. Wang and H. Fei, *J. Am. Chem. Soc.*, 2014, **136**, 17734–17737.
14 Y. You, S. Lee, T. Kim, K. Ohkubo, W. S. Chae, S. Fukuzumi, G. J. Jhon, W. Nam and S. J. Lippard, *J. Am. Chem. Soc.*, 2011, **133**, 18328–18342.
15 Y. You, Y. Han, Y. M. Lee, S. Y. Park, W. Nam and S. J. Lippard, *J. Am. Chem. Soc.*, 2011, **133**, 11488–11491.
16 L. He, C. P. Tan, R. R. Ye, Y. Z. Zhao, Y. H. Liu, Q. Zhao, L. N. Ji and Z. W. Mao, *Angew. Chem., Int. Ed.*, 2014, **53**, 12137–12141.
17 Y. Li, C. P. Tan, W. Zhang, L. He, L. N. Ji and Z. W. Mao, *Biomaterials*, 2015, **39**, 95–104.

18 L. He, Y. Li, C. P. Tan, R. R. Ye, M. H. Chen, J. J. Cao, L. N. Ji and Z. W. Mao, *Chem. Sci.*, 2015, **6**, 5409–5418.
19 R. R. Ye, C. P. Tan, L. He, M. H. Chen, L. N. Ji and Z. W. Mao, *Chem. Commun.*, 2014, **50**, 10945–10948.
20 R. A. Cairns, I. S. Harris and T. W. Mak, *Nat. Rev. Cancer*, 2011, **11**, 85–95.
21 J. R. Cantor and D. M. Sabatini, *Cancer Discovery*, 2012, **2**, 881–898.
22 W. H. Koppenol, P. L. Bounds and C. V. Dang, *Nat. Rev. Cancer*, 2011, **11**, 325–337.
23 P. S. Ward and C. B. Thompson, *Cancer Cell*, 2012, **21**, 297–308.
24 M. G. Vander Heiden, L. C. Cantley and C. B. Thompson, *Science*, 2009, **324**, 1029–1033.
25 S. E. Weinberg and N. S. Chandel, *Nat. Chem. Biol.*, 2014, **11**, 9–15.
26 S. W. Tait and D. R. Green, *Nat. Rev. Mol. Cell Biol.*, 2010, **11**, 621–632.
27 S. S. Sabharwal and P. T. Schumacker, *Nat. Rev. Cancer*, 2014, **14**, 709–721.
28 S. Fulda, L. Galluzzi and G. Kroemer, *Nat. Rev. Drug Discovery*, 2010, **9**, 447–464.
29 R. Kumar, J. Han, H. J. Lim, W. X. Ren, J. Y. Lim, J. H. Kim and J. S. Kim, *J. Am. Chem. Soc.*, 2014, **136**, 17836–17843.
30 R. Kumar, W. S. Shin, K. Sunwoo, W. Y. Kim, S. Koo, S. Bhuniya and J. S. Kim, *Chem. Soc. Rev.*, 2015, **44**, 6670–6683.
31 S. P. Wisnovsky, J. J. Wilson, R. J. Radford, M. P. Pereira, M. R. Chan, R. R. Laposa, S. J. Lippard and S. O. Kelley, *Chem. Biol.*, 2013, **20**, 1323–1328.
32 W. Zhou, X. Wang, M. Hu, C. Zhu and Z. Guo, *Chem. Sci.*, 2014, **5**, 2761–2770.
33 A. D. Presley, K. M. Fuller and E. A. Arriaga, *J. Chromatogr. B: Anal. Technol. Biomed. Life Sci.*, 2003, **793**, 141–150.
34 M. H. Lee, N. Park, C. Yi, J. H. Han, J. H. Hong, K. P. Kim, D. H. Kang, J. L. Sessler, C. Kang and J. S. Kim, *J. Am. Chem. Soc.*, 2014, **136**, 14136–14142.
35 S. J. Liu, Q. Zhao, Q. L. Fan and W. Huang, *Eur. J. Inorg. Chem.*, 2008, 2177–2185.
36 Y. You, S. Cho and W. Nam, *Inorg. Chem.*, 2014, **53**, 1804–1815.
37 K. K. Lo, *Acc. Chem. Res.*, 2015, **48**, 2985–2995.
38 J. S. Y. Lau, P. K. Lee, K. H. K. Tsang, C. H. C. Ng, Y. W. Lam, S. H. Cheng and K. K. W. Lo, *Inorg. Chem.*, 2009, **48**, 708–718.
39 G. L. Zhang, H. Y. Zhang, Y. Gao, R. Tao, L. J. Xin, J. Y. Yi, F. Y. Li, W. L. Liu and J. Qiao, *Organometallics*, 2014, **33**, 61–68.
40 C. A. Puckett and J. K. Barton, *J. Am. Chem. Soc.*, 2007, **129**, 46–47.
41 M. Poot, Y. Z. Zhang, J. A. Kramer, K. S. Wells, L. J. Jones, D. K. Hanzel, A. G. Lugade, V. L. Singer and R. P. Haugland, *J. Histochem. Cytochem.*, 1996, **44**, 1363–1372.
42 S. T. Smiley, M. Reers, C. Mottola-Hartshorn, M. Lin, A. Chen, T. W. Smith, G. D. Steele Jr and L. B. Chen, *Proc. Natl. Acad. Sci. U. S. A.*, 1991, **88**, 3671–3675.
43 D. A. Ferrick, A. Neilson and C. Beeson, *Drug Discovery Today*, 2008, **13**, 268–274.
44 M. Wu, A. Neilson, A. L. Swift, R. Moran, J. Tamagnine, D. Parslow, S. Armistead, K. Lemire, J. Orrell, J. Teich, S. Chomicz and D. A. Ferrick, *Am. J. Physiol.: Cell Physiol.*, 2006, **292**, C125–C136.
45 H.-Y. Lu, Y.-J. Chang, N.-C. Fan, L.-S. Wang, N.-C. Lai, C.-M. Yang, L.-C. Wu and J.-a. A. Ho, *Biomaterials*, 2015, **42**, 30–41.
46 S. A. Detmer and D. C. Chan, *Nat. Rev. Mol. Cell Biol.*, 2007, **8**, 870–879.
47 C. W. Leung, Y. Hong, S. Chen, E. Zhao, J. W. Lam and B. Z. Tang, *J. Am. Chem. Soc.*, 2013, **135**, 62–65.
48 H. Wang and J. A. Joseph, *Free Radical Biol. Med.*, 1999, **27**, 612–616.
49 H. M. McBride, M. Neuspiel and S. Wasiak, *Curr. Biol.*, 2006, **16**, R551–R560.
50 R. J. DeBerardinis, J. J. Lum, G. Hatzivassiliou and C. B. Thompson, *Cell Metab.*, 2008, **7**, 11–20.
51 R. S. Hotchkiss, A. Strasser, J. E. McDunn and P. E. Swanson, *N. Engl. J. Med.*, 2009, **361**, 1570–1583.
52 S. J. Riedl and Y. G. Shi, *Nat. Rev. Mol. Cell Biol.*, 2004, **5**, 897–907.
53 A. Parcellier, S. Gurbuxani, E. Schmitt, E. Solary and C. Garrido, *Biochem. Biophys. Res. Commun.*, 2003, **304**, 505–512.
54 D. W. Huang, B. T. Sherman and R. A. Lempicki, *Nat. Protoc.*, 2008, **4**, 44–57.
55 J. Lamb, E. D. Crawford, D. Peck, J. W. Modell, I. C. Blat, M. J. Wrobel, J. Lerner, J. P. Brunet, A. Subramanian, K. N. Ross, M. Reich, H. Hieronymus, G. Wei, S. A. Armstrong, S. J. Haggarty, P. A. Clemons, R. Wei, S. A. Carr, E. S. Lander and T. R. Golub, *Science*, 2006, **313**, 1929–1935.
56 W. Xiang, J. K. Cheong, S. H. Ang, B. Teo, P. Xu, K. Asari, W. T. Sun, H. Than, R. M. Bunte, D. M. Virshup and C. Chuah, *OncoTargets Ther.*, 2015, **6**, 33769–33780.